



HAL
open science

JWST/NIRCam Discovery of the First Y+Y Brown Dwarf Binary: WISE J033605.05–014350.4

Per Calissendorff, Matthew de Furio, Michael Meyer, Loïc Albert, Christian Aganze, Mohamad Ali-Dib, Daniella Bardalez Gagliuffi, Frederique Baron, Charles Beichman, Adam Burgasser, et al.

► **To cite this version:**

Per Calissendorff, Matthew de Furio, Michael Meyer, Loïc Albert, Christian Aganze, et al.. JWST/NIRCam Discovery of the First Y+Y Brown Dwarf Binary: WISE J033605.05–014350.4. The Astrophysical journal letters, 2023, 947 (2), pp.L30. 10.3847/2041-8213/acc86d . hal-04254064

HAL Id: hal-04254064

<https://hal.science/hal-04254064v1>

Submitted on 24 Oct 2023

HAL is a multi-disciplinary open access archive for the deposit and dissemination of scientific research documents, whether they are published or not. The documents may come from teaching and research institutions in France or abroad, or from public or private research centers.

L'archive ouverte pluridisciplinaire **HAL**, est destinée au dépôt et à la diffusion de documents scientifiques de niveau recherche, publiés ou non, émanant des établissements d'enseignement et de recherche français ou étrangers, des laboratoires publics ou privés.



Distributed under a Creative Commons Attribution 4.0 International License



JWST/NIRCam Discovery of the First Y+Y Brown Dwarf Binary: WISE J033605.05–014350.4

Per Calissendorff¹ , Matthew De Furio¹ , Michael Meyer¹ , Loïc Albert^{2,3} , Christian Aganze⁴ , Mohamad Ali-Dib^{3,5} , Daniella C. Bardalez Gagliuffi⁶ , Frederique Baron^{2,3} , Charles A. Beichman⁷ , Adam J. Burgasser⁴ , Michael C. Cushing⁸ , Jacqueline Kelly Faherty⁹ , Clémence Fontaine^{2,3} , Christopher R. Gelino¹⁰ , John E. Gizis¹¹ , Alexandra Z. Greenbaum¹² , J. Davy Kirkpatrick¹⁰ , Sandy K. Leggett¹³ , Frantz Martinache¹⁴ , David Mary¹⁴, Mamadou N'Diaye¹⁴ , Benjamin J. S. Pope^{15,16} , Thomas Roellig¹⁷ , Johannes Sahlmann¹⁸ , Anand Sivaramakrishnan^{9,19,20} , Daniel Peter Thorngren²¹ , Marie Ygouf⁷ , and Thomas Vandal^{2,3}

¹Department of Astronomy, University of Michigan, Ann Arbor, MI 48109, USA; percal@umich.edu

²Département de Physique and Observatoire du Mont-Mégantic, Université de Montréal, C.P. 6128, Succ. Centre-ville, Montréal, QC H3C 3J7, Canada

³Institut Trottiert de Recherche sur les exoplanètes, Université de Montréal, Québec, Canada

⁴University of California, San Diego, La Jolla, CA, USA

⁵Center for Astro, Particle and Planetary Physics (CAP3), New York University Abu Dhabi, UAE

⁶Department of Physics & Astronomy, Amherst College, 25 East Drive, Amherst, MA 01003, USA

⁷Jet Propulsion Laboratory, Pasadena, CA, USA

⁸Ritter Astrophysical Research Center, Department of Physics and Astronomy, University of Toledo, 2801 W. Bancroft Street, Toledo, OH 43606, USA

⁹Astrophysics Department, American Museum of Natural History, 79th Street at Central Park West, New York, NY 10024, USA

¹⁰California Institute of Technology, Pasadena, CA, USA

¹¹University of Delaware, Newark, DE, USA

¹²IPAC, Mail Code 100-22, Caltech, 1200 E. California Boulevard, Pasadena, CA 91125, USA

¹³NOIRLab—Gemini North, Hilo, HI, USA

¹⁴Université Côte d'Azur, Observatoire de la Côte d'Azur, CNRS, Laboratoire Lagrange, France

¹⁵School of Mathematics and Physics, The University of Queensland, St Lucia, QLD 4072, Australia

¹⁶Centre for Astrophysics, University of Southern Queensland, West Street, Toowoomba, QLD 4350, Australia

¹⁷NASA Ames Research Center, MS 245-6, Moffett Field, CA 94035, USA

¹⁸RHEA Group for the European Space Agency (ESA), European Space Astronomy Centre (ESAC), Camino Bajo del Castillo s/n, E-28692 Villanueva de la Cañada, Madrid, Spain

¹⁹Space Telescope Science Institute, 3700 San Martin Drive, Baltimore, MD 21218, USA

²⁰Department of Physics and Astronomy, Johns Hopkins University, 3701 San Martin Drive, Baltimore, MD 21218, USA

²¹Université de Montréal, Québec, Canada

Received 2023 March 10; revised 2023 March 27; accepted 2023 March 28; published 2023 April 25

Abstract

We report the discovery of the first brown dwarf binary system with a Y dwarf primary, WISE J033605.05–014350.4, observed with NIRCam on JWST with the F150W and F480M filters. We employed an empirical point-spread function binary model to identify the companion, located at a projected separation of $0''.084$, position angle of 295° , and with contrasts of 2.8 and 1.8 mag in F150W and F480M, respectively. At a distance of 10 pc based on its Spitzer parallax, and assuming a random inclination distribution, the physical separation is approximately 1 au. Evolutionary models predict for that an age of 1–5 Gyr, the companion mass is about 4–12.5 Jupiter masses around the 7.5–20 Jupiter mass primary, corresponding to a companion-to-host mass fraction of $q = 0.61 \pm 0.05$. Under the assumption of a Keplerian orbit the period for this extreme binary is in the range of 5–9 yr. The system joins a small but growing sample of ultracool dwarf binaries with effective temperatures of a few hundreds of Kelvin. Brown dwarf binaries lie at the nexus of importance for understanding the formation mechanisms of these elusive objects, as they allow us to investigate whether the companions formed as stars or as planets in a disk around the primary.

Unified Astronomy Thesaurus concepts: [Brown dwarfs \(185\)](#); [Y dwarfs \(1827\)](#); [James Webb Space Telescope \(2291\)](#)

1. Introduction

Brown dwarfs are cool substellar objects with masses below the $\approx 80 M_{\text{Jup}}$ hydrogen-burning limit (e.g., Burrows et al. 2001). Studies of the initial mass function for stars extend far into the substellar regime, even below $5 M_{\text{Jup}}$ (Kirkpatrick et al. 2019), which sets a tight boundary condition on the processes through which brown dwarfs can form. These formation processes may be similar to mechanisms that drive star

formation like gravitational collapse of giant molecular clouds, or analogous to those of giant planets through planetesimal growth in a circumstellar disk. Brown dwarfs could also form through entirely other modes such as ejection from star-forming aggregates (Reipurth & Clarke 2001).

Studies of the multiplicity of these objects is an efficient approach to constrain theories of their formation. Those studies can measure and constrain fundamental trends such as the orbital separation of binaries, a , as well as the companion-to-host mass ratio, $q \equiv M_{\text{B}}/M_{\text{A}}$. For stars the orbital separation distribution appears log-normal with a larger peak for higher-mass stars (e.g., Raghavan et al. 2010; De Rosa et al. 2014; Winters et al. 2019), so that the binary separation increases

Original content from this work may be used under the terms of the [Creative Commons Attribution 4.0 licence](#). Any further distribution of this work must maintain attribution to the author(s) and the title of the work, journal citation and DOI.

with mass. The companion mass ratio distribution also appears to change as a function of primary mass (Duchêne & Kraus 2013), changing from bottom heavy to top heavy for O stars to brown dwarfs respectively (Offner et al. 2022). Brown dwarf binaries appear to be consistent with the orbital radius trend observed for higher-mass multiples and typically form tighter orbital configurations. Burgasser et al. (2003, 2006) studied T0–T8 spectral types for binarity, finding all identified systems to have separations <5 au and mass ratios >0.8 , thus confirming the trend. Those early studies were however limited by only being sensitive to mass ratios >0.5 and did not probe the full range of mass ratios. More recent works have been able to complement this, confirming the trend over a larger range of $q=0.2-1$ and separations $a=0.1-1000$ au (Fontanive et al. 2018), hence extending previous works across virtually the full dynamic range of mass ratios and separations.

During the past decade we have seen an increase in the discoveries of brown dwarfs in the solar neighborhood, much to the efforts of deep imaging surveys and infrared missions such as the Wide-field Infrared Survey Explorer (WISE; Wright et al. 2010). Cushing et al. (2011) discovered several brown dwarfs from WISE data to have spectral features that distinguished them from the previously known latest T-type dwarfs, providing a clear transition to the identified Y dwarf spectral class. These Y dwarfs represent an extreme in temperature among the field star populations of the Milky Way (Cushing et al. 2011; Kirkpatrick et al. 2019; Zalesky et al. 2019), and can be used as probes to connect brown dwarfs and exoplanets (Beichman et al. 2014). They have effective temperatures lower than 500 K, with some approaching that of Jupiter (130 K; Hanel et al. 1981). For brown dwarfs, Coulomb and electron degeneracy effects compete in the equation of state, dictating their structure so that typical radii are close to that of Jupiter (Burrows et al. 2011). Thus, the range of temperatures results in a range of luminosities.

Y dwarfs are much brighter at wavelengths $>4.5 \mu\text{m}$ than at shorter wavelengths, so for these objects the Near Infrared Camera (NIRCam) on JWST is orders of magnitude more sensitive than any other facility and the ideal tool for studying Y dwarf multiplicity properties. As part of a JWST Cycle 1 GO program (#2473; Albert et al. 2021),²² we are conducting a survey of 20 Y dwarfs that is sensitive to companions beyond 1 au and down to $1 M_{\text{Jup}}$ given estimated sensitivity limits prelaunch (Ceau et al. 2019). Here we present our first discovery, a faint companion to the Y dwarf WISE J033605.05–014350.4 (hereafter W0336) and, therefore, the first Y+Y binary system.

2. Observations and Reduction

W0336 was first discovered by Kirkpatrick et al. (2012) using WISE data, and the unresolved system has been classified as a Y0 dwarf (Martin et al. 2018)²³ with an estimated effective temperature of $T_{\text{eff}} = 460 \pm 79$ K (Kirkpatrick et al. 2021). Spitzer (Werner et al. 2004) observations were used to measure the astrometry of the object (Martin et al. 2018; Kirkpatrick et al. 2019), and here we adopt the results from Kirkpatrick

et al. (2021) with a parallax of $\pi = 99.8 \pm 2.1$ mas and proper motions of $\mu_{\text{R.A.}} = -251.5 \pm 0.9$ mas yr⁻¹ and $\mu_{\text{decl.}} = -1216.1 \pm 0.93$ mas yr⁻¹.

We observed the target with JWST/NIRCam on 2022 September 22 at 12:49:44 UT, obtaining images in both F150W and F480M filters simultaneously. The source was observed with NIRCam imaging mode using a five-point subpixel Small-Grid-Dither pattern for a total exposure time of 2630.509 s with the BRIGHT1 readout pattern. The data were reduced by the official JWST pipeline with the data-processing software version 2022_3a, and downloaded from the MAST archive based on calibration software version 1.7.2.²⁴ The unresolved photometry of the system was estimated using the photutils Python package (Bradley et al. 2022) and the JWST photometric reference data *jwst_nircam_photom_0114.fits*. An aperture size equal to 70% encircled energy was adopted together with appropriate aperture corrections in accordance with the JWST Calibration Reference Data System. We employed our analysis on the intermediate data reduction step, level 2 pipeline product **cal.fits* files, further described in Section 3. In addition to the standard calibrated images we performed our own background subtraction by fitting an annulus with a 10–15 pixel radius centered upon the target.

We verified the positions of the target W0336 for the two bands by overplotting their respective images. The images from each band are shown in Figure 1, illustrating that W0336 appears brighter in the longer-wavelength band F480M. The images have been rotated with respect to the instrument aperture positional angle (NIRCam APA) of 271°.61 in the F150W band and 270°.79 in the F480M band at the time of the observations, so that north is up and east is to the left in the images. We also cross-referenced the position of W0336 with publicly available Hubble Space Telescope images from GO-16229²⁵ in the F160W filter, verifying the position and motion of the system compared to background sources.

3. Empirical Point-spread Function Analysis

In order to search for companions at small separations, we applied a binary point-spread function (PSF) fitting routine using empirically derived PSF models, thoroughly described in De Furio et al. (2023). This analysis was based on the empirical PSF (ePSF) construction described by Anderson & King (2000) and has been applied to find close companions on subpixel scales using, for example, Hubble Space Telescope images (De Furio et al. 2019, 2022a, 2022b).

We constructed the ePSF for each filter using three other Y dwarfs that were observed close in time to W0336 (WISE J035934.06–540154.6, WISE J030449.03–270508.3, and WISE J041022.71+150248.4), within a 36 hour window. We used a pixel box size of 11×11 pixels centered upon the flux peak of the selected sources and constructed a $4 \times$ oversampled PSF model. Each source was observed with a pattern of five subpixel dither positions, allowing for more detailed subpixel modeling of the ePSF. All dither positions were used in the making of the ePSF for a total of $3 \times 5 = 15$ sources for the final combined ePSF in each filter. The PSF for a relatively wide bandpass can vary between objects if those objects have

²² <https://www.stsci.edu/jwst/phase2-public/2473.pdf>

²³ Some discrepancies have been reported in the W0336 spectral type, likely related to a low signal-to-noise ratio of the observed spectrum (Mace et al. 2013; Martin et al. 2018).

²⁴ Using calibration reference data system version 11.16.14 with the reference file *jwst_1023.pmap*.

²⁵ <https://www.stsci.edu/hst/phase2-public/16229.pdf>

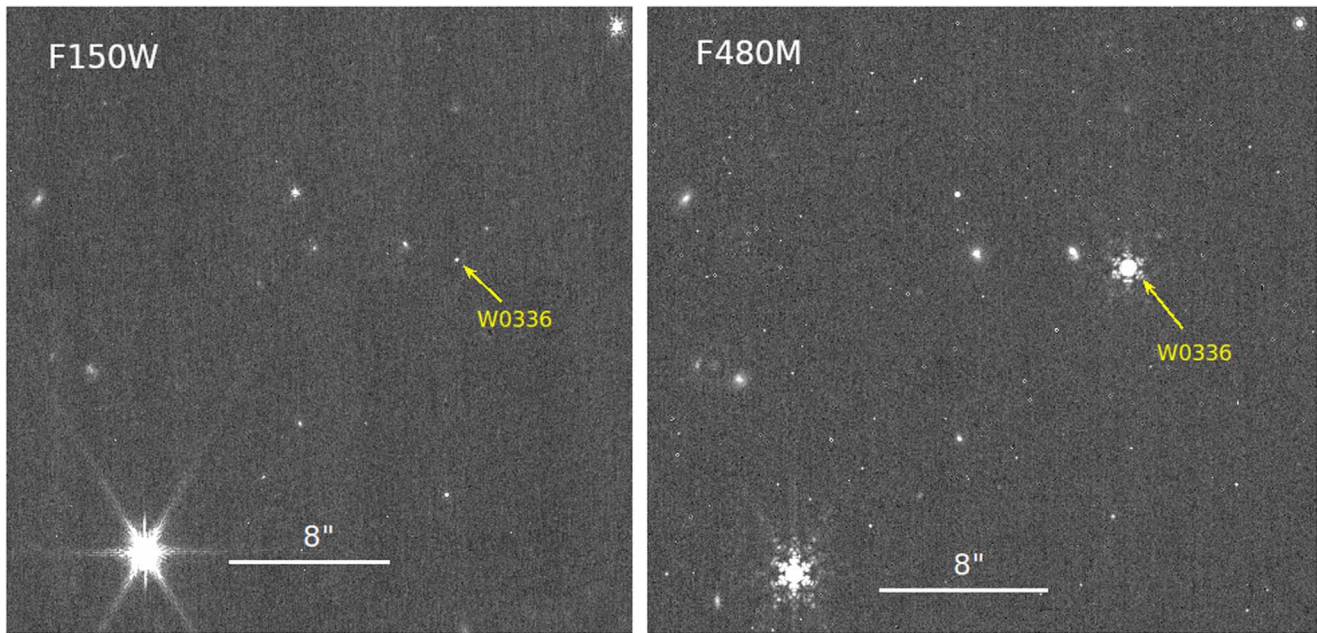


Figure 1. JWST/NIRCam images showing the aligned and scaled images of the target W0336 in each observed filter. North is up and east is to the left in the images.

different spectral energy distributions through the filter. We therefore chose these sources to ensure consistent color to retain the integrity of the expected PSF of a Y dwarf and to minimize wave front error drifts over a short amount of time in order to optimize our estimation of the astrophysical scene.

We then used the ePSF to fit both single and double PSF models to the Y dwarf data. We employed a Nested Sampling routine using the PyMultiNest Python package (Buchner et al. 2014) that performs the Nested Sampling Monte Carlo analysis using MultiNest (Feroz et al. 2009). Our single model consists of three parameters: x and y center position and flux normalization of the target source. Our binary model consists of six parameters: x and y center of the primary, flux normalization of the primary, separation between the centers of the primary and secondary, the position angle of the center of the secondary relative to the primary, and the flux ratio between the secondary and primary ($f_r \equiv f_B/f_A$). The priors to the primary coordinates were set as flat over ± 1.5 pixels from the center of the pixel box. The companion parameter priors were set as flat over separations between 0.5 and 5.0 pixels, as we do not expect to be sensitive to companions closer in than half a pixel, and we limited the search to the size of the pixel box. The positional angle prior was set to be flat between 0° and 360° and the flux ratio prior was log-uniform over 10^{-4} –1.

PyMultiNest calculates the Bayesian evidence of the model, which we used to determine whether a binary or single model fits the data better. We first fit each dither position individually to ensure that the companion was detected in every image, while also verifying consistency, and check for possible bad frames. We then fit all dither positions simultaneously, treating the x - and y -positions of the primary as free parameters for each dither position, while keeping the parameters for the secondary component the same for all dithers, for a total of 14 parameters to be varied in the binary model fit. Figure 2 displays the data images, model systems, and corresponding residuals for the different cases in the F480M filter, and the best-fit values for both filters are presented in Table 1.

4. Results and Discussion

The empirical PSF analysis provides a compelling first look at these data. This is the only companion found with this method in our sample of 12 Y dwarfs observed to date and is the first companion ever discovered around a Y dwarf primary. Although these are low number statistics, the observed frequency of companions in our sample (1/12) is consistent with the companion frequency to late T dwarfs (8%) over mass ratios of $q = 0.2$ –1.0 and separations of $a = 0.1$ –1000 au (e.g., Fontanive et al. 2018). Future work will characterize the companion population and estimate the companion frequency over mass ratios and orbital separations sampled across our entire survey.

Table 1 gives the angular separation and orientation of the resolved system. The values are estimated from the median of the probability density function obtained from the multinested Monte Carlo approach, with errors being the 16th and 84th percentiles. The separation measured in pixels is converted into milliarcseconds using the nominal plate scale from the JWST user documentation²⁶ of $63 \text{ mas pixel}^{-1}$ and $31 \text{ mas pixel}^{-1}$ for the F480M and F150W filters, respectively. We adopt the angular separation of $0''.084$ measured in the F480M filter where the companion is brighter. Given the distance of $10.02 \pm 0.21 \text{ pc}$ from the Spitzer parallax, the estimated separation corresponds to a projected separation of $0.89^{+0.07}_{-0.10} \text{ au}$. This separation is consistent with what one would expect given the orbital separation distribution from Fontanive et al. (2018) for late T and early Y dwarfs with a peak at $2.9^{+0.8}_{-1.4} \text{ au}$ in projected separation. The probability of the companion being a background contamination is extremely low given its proximity to the primary. Assuming a randomly uniform distribution of objects brighter than the companion W0336B in the field of view of our NIRCam images, we obtain a probability of $\sim 4 \times 10^{-6}$ for a chance projection at the same separation as the discovered companion.

²⁶ <https://jwst-docs.stsci.edu/jwst-near-infrared-camera>

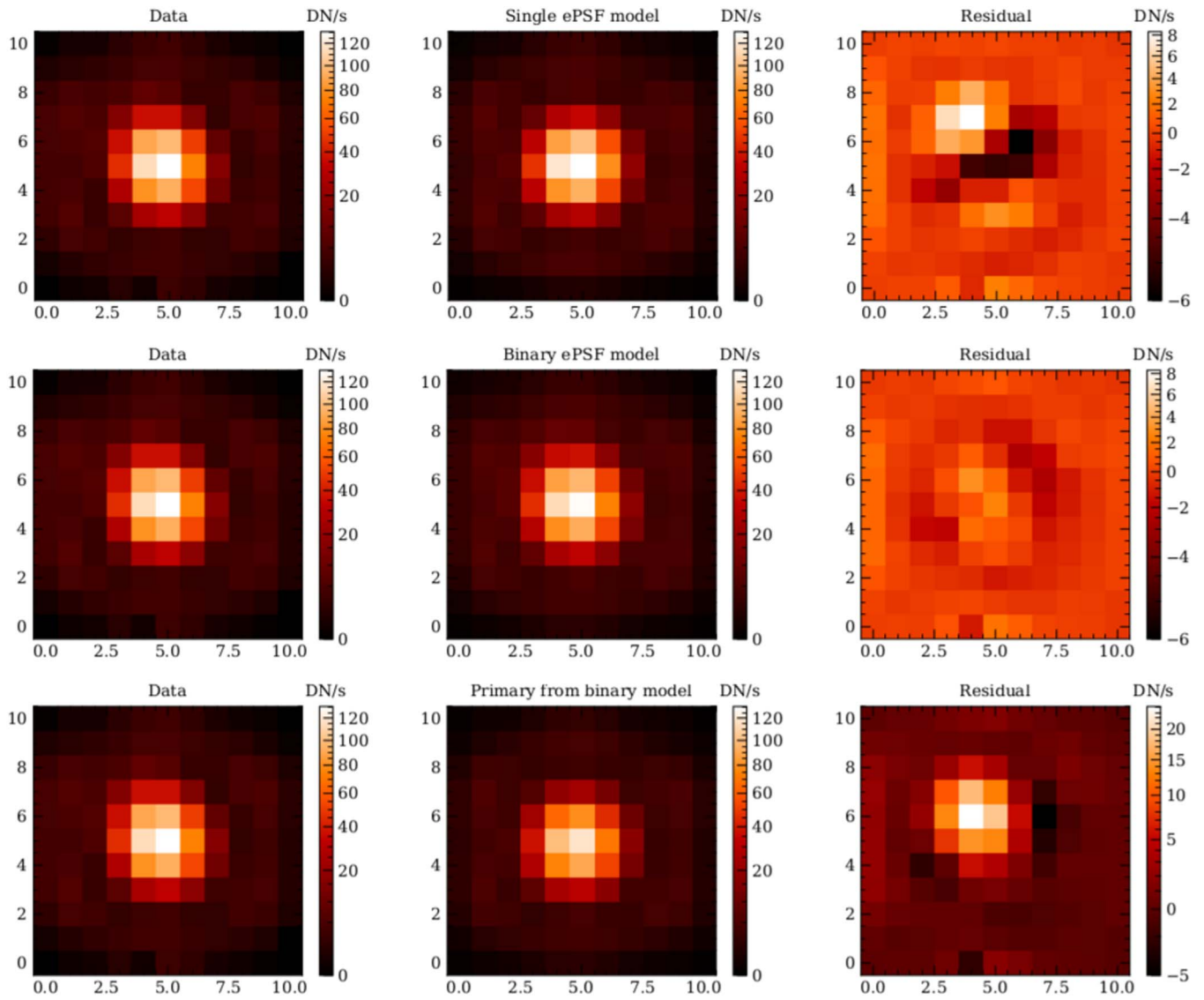


Figure 2. Images displaying the pipeline calibrated data of W0336 in the F480M band are in the left column, models are in the middle column, and their corresponding residuals when the models have been subtracted from the data are in the right column. The top row shows a single model fitted to the data, and the middle row shows a binary double ePSF model. The bottom row depicts the same binary model as the middle row, but only showing the primary component from that fit to better highlight the companion seen in the residuals after subtracting the primary component from the data. The units are in DN/s. The color scheme in the images are scaled to a power law with an exponent of 0.5, and the color bar for the binary model residual image has been scaled to match the single model residual image to better highlight the smaller residual and improved fit.

Table 1 also gives the measured F150W and F480M Vega magnitudes for the unresolved system and for the resolved components, where the resolved magnitudes are calculated from our contrast measurements of flux ratio between the components. Figure 3 shows a color–magnitude diagram for the system, together with model sequences. There are two recent model families that apply cloud-free atmospheres and cover the low luminosities of the W0336 system—the Sonora Bobcat models (Marley et al. 2021) and the ATMO2020 models (Phillips et al. 2020; Leggett et al. 2021). The ATMO2020 models include disequilibrium chemistry and a physically motivated empirical adjustment to the atmosphere’s pressure–temperature profile (see discussion in Leggett et al. 2021). Figure 3 shows that the two model sets predict very similar values of M_{F150W} for a given T_{eff} and gravity, although the F150W–F480M colors can differ. The models are thus expected to provide reliable estimates of T_{eff} for the W0336

system, given in Table 1. The uncertainties in T_{eff} have been estimated from the range of M_{F150W} values calculated by the models for plausible ranges in gravity and metallicity (Table 9 of Leggett et al. 2021).

There are no constraints on age for this isolated system. However, studies of the solar neighborhood, and of low-mass stars and brown dwarfs in particular, suggest a likely age range for this system of 1–3 Gyr (e.g., Dupuy & Liu 2017). The ATMO2020 models and Figure 3 on the other hand suggest that the age of the system may be older than 5 Gyr and also that the system has approximately solar metallicity (not shown). However, the uncertainty in the measured F150W–F480M colors, and systematic differences in the models, means that surface gravity cannot be fully constrained, which would have in turn constrained mass and hence age.

Nevertheless, Table 1 gives estimates of mass for the W0336 components for ages of 1 and 5 Gyr, derived from our absolute

Table 1
Properties of the W0336 Binary System

Band	F150W	F480M
Separation [mas]	$89.8^{+3.8}_{-4.1}$	$83.7^{+4.9}_{-8.2}$
Position angle [deg]	299.1 ± 3.4	$295.4^{+2.3}_{-2.6}$
Contrast [mag]	$2.82^{+0.19}_{-0.11}$	$1.81^{+0.14}_{-0.31}$
W0336AB	21.97 ± 0.01	14.52 ± 0.01
W0336A	22.05 ± 0.01	$14.71^{+0.02}_{-0.05}$
W0336B	$24.87^{+0.18}_{-0.10}$	$16.51^{+0.12}_{-0.26}$
Component	Primary	Secondary
T_{eff} [K]	415 ± 20	325^{+15}_{-10}
M [M_{Jup}] (1 Gyr)	8.5 ± 1	5 ± 1
M [M_{Jup}] (5 Gyr)	18 ± 2	11.5 ± 1
Physical separation [au]	$0.97^{+0.05}_{-0.09}$	
Orbital period [yr]	7 ± 2	
Mass fraction $q = M_B/M_A$	0.61 ± 0.05	

magnitude estimates and the Sonora evolutionary models (Marley et al. 2021). The mass estimates range from 7.5 to $20.0 M_{\text{Jup}}$ for the primary and 4.0 to $12.5 M_{\text{Jup}}$ for the secondary, and the mass ratio of the system is around $q = 0.6$, at the low end of the distribution found for low-mass binaries with masses $\leq 40 M_{\text{Jup}}$ inferred from Lyon/COND models (Fontanive et al. 2018). Interestingly, W0336B appears to lie at or below the deuterium-burning limit of $13 M_{\text{Jup}}$, sometimes used as a boundary between brown dwarfs and planets (Spiegel et al. 2011). If the system is 2 Gyr old or younger, both components lie below this limit. In any case, the companion joins a growing list of cold brown dwarfs and isolated young brown dwarfs that may serve as a constraint on the minimum mass for opacity limited fragmentation.

Applying the conversion factor of 1.16 between projected and physical orbits from Dupuy & Liu (2011) for isotropic randomly distributed inclinations with the measured distance, we find the W0336 binary to be separated by $0.97^{+0.05}_{-0.09}$ au. Combining this with the mass range from the evolutionary models, a tentative orbital period can be estimated for the system of 5–6 yr in the higher system mass scenario and 7–9 yr in the lower system mass case. A dynamical mass from orbital monitoring could thus be obtained in a relatively short time span for the system. The system is far too faint for Gaia to observe any astrometric acceleration that could otherwise aid in placing dynamical mass constraints.

Among the few brown dwarf binaries where the primary has a spectral type of T8 or later, few have been reported to be low- q systems: WISEPC J121756.91+162640.2 (T9+Y0, 12+8 M_{Jup}) and WISEPA J171104.60+350036.8 (T8+T9.5, 20+9 M_{Jup}) (Liu et al. 2012). However, both these systems have much larger separations of ~ 8 –15 au and break from the expected orbital distribution trend otherwise observed. Dupuy et al. (2015) reported on the T+Y dwarf binary WISE J014656.66+423410.0, with a similar projected separation to W0336 of $0.93^{+0.16}_{-0.12}$ au, albeit with a higher mass-ratio $q \geq 0.9$. That W0336 in contrast is a tightly bound system with a low mass-ratio is an intriguing discovery. With the low number statistics for these extreme systems it is unclear whether they represent the true binary population of ultracool dwarfs or can be considered as peculiar systems. It is also possible that many systems go undetected where the separation is too tight for them to be retrieved. Indeed, W0336 confirms that late-type

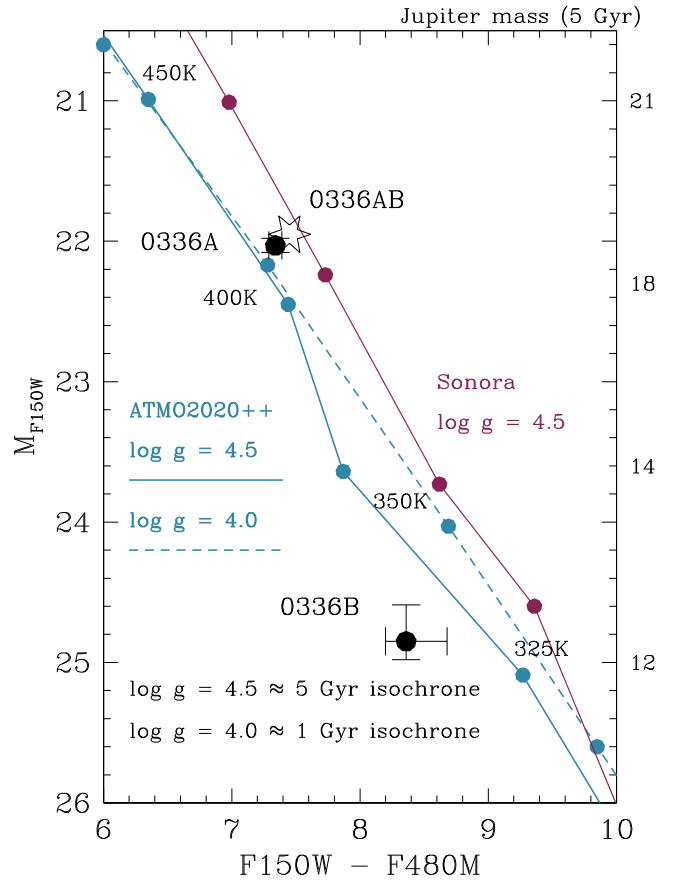


Figure 3. Color–magnitude diagram for W0336 in the NIRCcam filters used in this work. The open star corresponds to the unresolved system, and the black filled points indicate the resolved components. Model sequences are shown for effective temperatures, and surface gravities are indicated in the legend. All models are for cloud-free solar metallicity atmospheres; however, the Sonora models (Marley et al. 2021) are in chemical equilibrium, while the ATMO2020++ models (Phillips et al. 2020; Leggett et al. 2021) include disequilibrium chemistry and also an adjusted pressure–temperature profile. The masses along the right axis are taken from the Sonora evolutionary models of Marley et al. (2021), for $\log g = 4.5$, and the temperatures are indicated along the sequences.

and low-mass binaries exist and survive in tight configurations, and surveys approaching sub-astronomical-unit separations are needed to discover them. Such endeavors could be taken using, for example, kernel phase interferometry (Ceau et al. 2019).




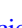
Follow-up spectroscopic and photometric observations over a wide wavelength range are needed to further constrain the properties of both the primary and its companion. Substellar binaries on small separations such as these can be resolved with, for example, integral field units to obtain valuable spectral information (e.g., Calissendorff et al. 2019). Such multiple pairs, assuming a common formation age and composition, represent critical constraints on atmospheric as well as evolutionary theory of the formation and evolution of substellar companions.

We thank the reviewer for the constructive comments. This work is based on observations made with the NASA/ESA/CSA James Webb Space Telescope. The data were obtained from the Mikulski Archive for Space Telescopes at the Space Telescope Science Institute, which is operated by the Association of Universities for Research in Astronomy, Inc., under NASA contract NAS 5-03127 for JWST. These observations are associated with program #2473 and can be accessed via

doi:10.17909/9zgc-m183. Support for program #2743 was provided by NASA through a grant from the Space Telescope Science Institute, which is operated by the Association of Universities for Research in Astronomy, Inc., under NASA contract NAS 5-03127. L.A. acknowledges support of the Canadian Space Agency through contract 22JWGO1-11. T.L.R. would like to acknowledge the support of the NASA Science Mission Directorate under WBS 411672.07.05.05.03.01. This work was authored by employees of Caltech/IPAC under Contract No. 80GSFC21R0032 with the National Aeronautics and Space Administration.

ORCID iDs

Per Calissendorff  <https://orcid.org/0000-0002-5335-0616>
 Matthew De Furio  <https://orcid.org/0000-0003-1863-4960>
 Michael Meyer  <https://orcid.org/0000-0003-1227-3084>
 Loïc Albert  <https://orcid.org/0000-0003-0475-9375>
 Christian Aganze  <https://orcid.org/0000-0003-2094-9128>
 Mohamad Ali-Dib  <https://orcid.org/0000-0002-6633-376X>
 Daniella C. Bardalez Gagliuffi  <https://orcid.org/0000-0001-8170-7072>
 Frederique Baron  <https://orcid.org/0000-0002-5074-1128>
 Charles A. Beichman  <https://orcid.org/0000-0002-5627-5471>
 Adam J. Burgasser  <https://orcid.org/0000-0002-6523-9536>
 Michael C. Cushing  <https://orcid.org/0000-0001-7780-3352>
 Jacqueline Kelly Faherty  <https://orcid.org/0000-0001-6251-0573>
 Clémence Fontanive  <https://orcid.org/0000-0002-2428-9932>
 Christopher R. Gelino  <https://orcid.org/0000-0001-5072-4574>
 John E. Gizis  <https://orcid.org/0000-0002-8916-1972>
 Alexandra Z. Greenbaum  <https://orcid.org/0000-0002-7162-8036>
 J. Davy Kirkpatrick  <https://orcid.org/0000-0003-4269-260X>
 Sandy K. Leggett  <https://orcid.org/0000-0002-3681-2989>
 Frantz Martinache  <https://orcid.org/0000-0003-1180-4138>
 Mamadou N'Diaye  <https://orcid.org/0000-0002-1721-3294>
 Benjamin J. S. Pope  <https://orcid.org/0000-0003-2595-9114>
 Thomas Roellig  <https://orcid.org/0000-0002-6730-5410>
 Johannes Sahlmann  <https://orcid.org/0000-0001-9525-3673>

Anand Sivaramakrishnan  <https://orcid.org/0000-0003-1251-4124>
 Daniel Peter Thorngren  <https://orcid.org/0000-0002-5113-8558>
 Marie Ygouf  <https://orcid.org/0000-0001-7591-2731>
 Thomas Vandal  <https://orcid.org/0000-0002-5922-8267>

References

- Anderson, J., & King, I. R. 2000, *PASP*, **112**, 1360
 Albert, L., Meyer, M. R., Ali-Dib, M., et al. 2021, JWST Proposal Cycle 1, ID #2473
 Beichman, C., Gelino, C. R., Kirkpatrick, J. D., et al. 2014, *ApJ*, **783**, 68
 Bradley, L., Sipőcz, B., Robitaille, T., et al. 2022, *astropy/photutils*: 1.5.0, Zenodo, doi:10.5281/zenodo.6825092
 Buchner, J., Georgakakis, A., Nandra, K., et al. 2014, *A&A*, **564**, A125
 Burgasser, A. J., Kirkpatrick, J. D., Cruz, K. L., et al. 2006, *ApJS*, **166**, 585
 Burgasser, A. J., Kirkpatrick, J. D., Reid, I. N., et al. 2003, *ApJ*, **586**, 512
 Burrows, A., Heng, K., & Nampaisarn, T. 2011, *ApJ*, **736**, 47
 Burrows, A., Hubbard, W. B., Lunine, J. I., et al. 2001, *RvMP*, **73**, 719
 Calissendorff, P., Janson, M., Asensio-Torres, R., et al. 2019, *A&A*, **627**, A167
 Ceau, A., Mary, D., Greenbaum, A., et al. 2019, *A&A*, **630**, A120
 Cushing, M. C., Kirkpatrick, J. D., Gelino, C. R., et al. 2011, *ApJ*, **743**, 50
 De Furio, M., Lew, B. W., Beichman, C. A., et al. 2023, arXiv:2302.12723
 De Furio, M., Liu, C., Meyer, M. R., et al. 2022b, *ApJ*, **941**, 161
 De Furio, M., Meyer, M. R., Reiter, M., et al. 2022a, *ApJ*, **925**, 112
 De Furio, M., Reiter, M., Meyer, M. R., et al. 2019, *ApJ*, **886**, 95
 De Rosa, R. J., Patience, J., Wilson, P. A., et al. 2014, *MNRAS*, **437**, 1216
 Duchêne, G., & Kraus, A. 2013, *ARA&A*, **51**, 269
 Dupuy, T. J., & Liu, M. C. 2011, *ApJ*, **733**, 122
 Dupuy, T. J., & Liu, M. C. 2017, *ApJS*, **231**, 15
 Dupuy, T. J., Liu, M. C., & Leggett, S. K. 2015, *ApJ*, **803**, 102
 Feroz, F., Hobson, M. P., & Bridges, M. 2009, *MNRAS*, **398**, 1601
 Fontanive, C., Biller, B., Bonavita, M., et al. 2018, *MNRAS*, **479**, 2702
 Hanel, R., Conrath, B., Herath, L., et al. 1981, *JGR*, **86**, 8705
 Kirkpatrick, J. D., Gelino, C. R., Cushing, M. C., et al. 2012, *ApJ*, **753**, 156
 Kirkpatrick, J. D., Gelino, C. R., Faherty, J. K., et al. 2021, *ApJS*, **253**, 7
 Kirkpatrick, J. D., Martin, E. C., Smart, R. L., et al. 2019, *ApJS*, **240**, 19
 Leggett, S. K., Tremblin, P., Phillips, M. W., et al. 2021, *ApJ*, **918**, 11
 Liu, M. C., Dupuy, T. J., Bowler, B. P., et al. 2012, *ApJ*, **758**, 57
 Mace, G. N., Kirkpatrick, J. D., Cushing, M. C., et al. 2013, *ApJS*, **205**, 6
 Marley, M. S., Saumon, D., Visscher, C., et al. 2021, *ApJ*, **920**, 85
 Martin, E. C., Kirkpatrick, J. D., Beichman, C. A., et al. 2018, *ApJ*, **867**, 109
 Offner, S. S. R., Moe, M., Kratter, K. M., et al. 2022, arXiv:2203.10066
 Phillips, M. W., Tremblin, P., Baraffe, I., et al. 2020, *A&A*, **637**, A38
 Raghavan, D., McAlister, H. A., Henry, T. J., et al. 2010, *ApJS*, **190**, 1
 Reipurth, B., & Clarke, C. 2001, *AJ*, **122**, 432
 Spiegel, D. S., Burrows, A., & Milsom, J. A. 2011, *ApJ*, **727**, 57
 Werner, M. W., Roellig, T. L., Low, F. J., et al. 2004, *ApJS*, **154**, 1
 Winters, J. G., Henry, T. J., Jao, W.-C., et al. 2019, *AJ*, **157**, 216
 Wright, E. L., Eisenhardt, P. R. M., Mainzer, A. K., et al. 2010, *AJ*, **140**, 1868
 Zalesky, J. A., Line, M. R., Schneider, A. C., et al. 2019, *ApJ*, **877**, 24